AAPS PharmSciTech (2022) 23: 89
DOI: 10.1208/s12249-022-02241-9

Research Article

Theme: Novel Advances in 3-D Printing Technology in Drug Delivery

In Vitro and *In Vivo* Evaluations of Berberine-Loaded Microparticles Filled In-House 3D Printed Hollow Capsular Device for Improved Oral Bioavailability

Dinesh Choudhury,[1,2] Aishwarya Jala,[3] Upadhyayula Suryanarayana Murty,[2,4] Roshan M. Borkar,[3] and Subham Banerjee[1,2,5]

Received 19 November 2021; accepted 19 February 2022; published online 16 March 2022

Abstract. The low oral bioavailability, short biological half-life, high dose, and frequent dosing of berberine (BBR) contribute to its restricted clinical use despite its extensive pharmacological activity. Thus, the objective of this study was to formulate sustained-release microparticles (MPs) using a pH-independent release polymer and to evaluate their potential to improve the oral bioavailability of BBR. BBR loaded MPs were prepared using the emulsion crosslinking method and evaluated for particle size, circularity, morphology, entrapment efficiency, solid-state analysis, swelling index, and *in vitro* BBR release study fitted with different models of release kinetics. The MPs exhibited desired particle sizes ranges between 11.09–11.62 μm and were almost spherical in shape, as confirmed by the circularity value and micrographic images. A loss of BBR crystallinity was observed after encapsulation in MPs, as evident from various solid-state analyses. The final optimized batch (F3) showed highest % BBR entrapment efficiency value of 81.63% ± 4.9. *The in vitro* BBR release performance in both acidic and alkaline media showed the desired sustained release behavior from the crosslinked MPs, where the maximum BBR release was observed at alkaline pH, which is in accordance with the swelling study data. In the *in vivo* study, the oral absorption profiles of BBR from both pristine and MPs formats were investigated using in-house prototyped 3D printed hollow capsules as a unit dose carrier. *In vivo* data showed sustained and prolonged absorption behavior of BBR from MPs compared to their pristine counterparts, which resulted in a cumulative increment of relative oral bioavailability to mitigate the aforementioned issues related to BBR.

KEY WORDS: berberine; microparticles; 3D printing; hollow capsular device; oral delivery.

INTRODUCTION

In the twenty-first century, drug discovery and development have continuously focused on natural chemical entities or plant metabolites. Berberine (BBR) is an active alkaloid found in several plants belonging to the family Berberidaceae, Annonaceae, Papaveraceae, Ranunculaceae, Rutaceae, and Menispermaceae (1). BBR has been widely used as a herbal drug for the treatment of numerous diseases since ancient times. BBR has been used in Chinese and Vietnamese traditional medicine, folk medicine in Iran, and Indian Ayurvedic medicine for decades (2, 3). Nevertheless, BBR is now chemically synthesized for clinical purposes, in which chloride or sulfate salts are mostly used (4).

It is mostly used against several microbial infections and to treat diarrhea, owing to its antimicrobial and anti-motility activities through its inhibitory action on the enzymatic or endotoxic activities of microorganisms (5, 6). Various experimental pharmacological and clinical studies have revealed that BBR has a decent therapeutic effect on most physiological systems in the human body (7). BBR has been used in several clinical trials for diseases such as diabetes, polycystic ovarian syndrome, postmenopausal osteoporosis, metabolic syndrome, atherosclerosis, congestive heart failure, hyperlipidemia, cancer, diarrhea, nonalcoholic fatty liver disease, bacterial infection, renal disease, and ophthalmic disease (3). From various pharmacological studies, approximately 90 biological targets of BBR have been identified (8). From numerous pharmacological activities, BBR showed extensive therapeutic effects against several neglected tropical diseases,

[1] Department of Pharmaceutics, National Institute of Pharmaceutical Education & Research (NIPER)-Guwahati, Changsari, Assam, India.
[2] National Centre for Pharmacoengineering, NIPER-Guwahati, Changsari, Assam, India.
[3] Department of Pharmaceutical analysis, NIPER-Guwahati, Changsari, Assam, India.
[4] NIPER-Guwahati, Changsari, Assam, India.
[5] To whom correspondence should be addressed. (e–mail: banerjee.subham@yahoo.co.in)

including leishmaniasis, lymphatic filariasis, scabies, schistosomiasis, dengue, chikungunya, trachoma, and other microbial and helminth-based neglected diseases (9–13). Hence, multiple neglected diseases can be therapeutically addressed by using a single compound. A recent *in silico* study showed that BBR displays a higher degree of interaction with viral proteases and hence can be used against SARS-CoV-2 (14).

Despite its extensive pharmacological effects, the clinical application of BBR is limited owing to its poor oral bioavailability. Owing to its lower aqueous solubility, BBR showed decreased absorption in the gastrointestinal tract (GIT); hence, the required plasma concentration was not achieved. The extensive first-pass effect and P-gp efflux with high extraction and distribution in the liver are key hindrances to the oral delivery of BBR (15, 16). In addition, BBR tends to self-aggregate in both gastric and intestinal media, which inhibits its dissolution in the GIT medium (17). The absolute bioavailability of BBR after oral administration was found to be less than 1.0% (18), and it was also determined that oral administration of BBR at a dose of 400 mg/kg resulted in a maximum plasma concentration (C_{max}) of 0.4 ng/mL (19). Because of these outcomes, high and frequent dosing is recommended for clinical applications. Such high doses can trigger adverse gastrointestinal reactions. These criticisms have restricted the development and use of BBR in pharmaceutical formulations for clinical applications. A probable solution to address these hindrances of BBR for clinical utilization is to adopt a controlled therapeutic strategy that will compensate for these deficits. Therefore, development of a sustained-release formulation with enhanced oral bioavailability is necessary for the therapeutic use of BBR. Sustained-release formulations of drugs can provide a smooth, controlled plasma concentration-time profile that enables effective oral administration of drugs and reduces the dosing frequency of such drugs (20).

Microparticle-based formulations are based on multiparticulate drug delivery systems in which drugs are administered *via* different routes with therapeutic and technological advantages. Microparticles (MPs) have several advantages, such as protection of drugs from the harsh gastrointestinal environment, masking of the bitter taste of drugs, preservation of volatile substances by encapsulation into the core, sustained and delayed release of drugs, and enhancement of the solubility and bioavailability of drugs (21). MPs enable amorphization of the drug after encapsulation in a polymeric matrix owing to molecular dispersion, resulting in an enhanced dissolution rate of the drug (22). The release of drugs from polymeric MPs depends on polymer properties. If the polymer undergoes erosion, the encapsulated drug diffuses through channels formed by breaking the polymer chains (23). Polymeric MPs also undergo swelling, and the drug diffuses through the pores formed by water. With the appropriate selection of polymers, MPs can be prepared and used in immediate, sustained, and delayed drug delivery systems (24). Upon oral administration, MPs spread homogenously in the GIT; as a result, the drug is released uniformly at a controlled rate, which improves the plasma concentration of the drug and avoids the burst release of the drug, which arises with the conventional formulation (25).

As BBR is considered to remain stable under all pH conditions in the GIT (26), a pH-independent polymer was selected for the preparation of BBR-loaded MPs. Kollicoat® SR 30 D is an aqueous dispersion of polyvinyl acetate with povidone and sodium lauryl sulfate as stabilizers, which is used mostly in pH-independent sustained-release delivery systems. Kollicoat® SR 30 D is widely used in the film coating of tablets owing to its excellent film-forming characteristics and mechanical properties. It has been widely used as a coating polymer in tablets (27), pellets (28), and granules (29) for the sustained release of drugs, as a matrix former (30) and to prevent the bitter taste of drugs (31). The mechanism of drug release from the Kollicoat® SR 30 D matrix involves swelling and diffusion (32).

For the administration of a unit dose of MPs, they can be incorporated into solid dosage forms such as tablets (33) or filled in capsules (34) and dispersed in liquid for parenteral applications. As Kollicoat® SR 30 D-MPs can release the drug in the GIT irrespective of pH, the capsules needed to break or dissolve in acidic pH to deliver the MPs. Hence, to deliver a unit dose of MPs, a capsular device was prototyped in-house in our laboratory *via* fused deposition modeling (FDM)-mediated 3D printing technology (Ultimaker 3, Ultimaker, Netherlands), as per our previous report (35). 3D printed capsules were printed in two parts, that is, the body and cap, according to their specific dimensions (size 00). The *in vitro release* of MPs from the fabricated 3D printed hollow capsular device was assessed in acidic medium.

Thus, the objective of this study was to fabricate pH-independent sustained-release BBR-MPs to improve their oral relative bioavailability (RBA). MPs were fabricated using the emulsion crosslinking method with two variables and further analyzed for particle size, circularity, entrapment, morphology, solid-state analysis, and *in vitro* BBR release studies. In addition, to administer a unit dose of MPs, a 3D printed hollow capsular device was utilized. Based on the *in vitro* performance, the best optimized batch of BBR-MPs was selected for *the in vivo* pharmacokinetic study, where both pristine BBR and BBR-MPs were filled inside the in-house prototyped 3D printed capsule (size 03) and administered *via* the oral route for comparison with RBAs.

MATERIALS AND METHODS

Materials

BBR (purity ≥98%), Kollicoat® SR 30 D, and glutaraldehyde solution (GA, 25% in water) were purchased from Sigma-Aldrich Chemical Co., St. Louis, MO, USA. Light-liquid paraffin and glycine were obtained from Loba Chemie Pvt. Ltd., and HiMedia Laboratories Pvt. Ltd., respectively. Palmatine chloride, which was used as the internal standard, was purchased from Sigma-Aldrich Chemical Co., St. Louis, MO, USA. All other reagents were of analytical grade. Milli-Q water was used for all the experiments.

Preparation of MPs

MPs were prepared using an emulsion crosslinking method, in which GA was used as a crosslinker (36). Kollicoat® SR 30 D, a polymeric dispersion of polyvinyl acetate stabilized with polyvinylpyrrolidone and sodium lauryl sulfate in water, was used as the matrix to form the MPs. MPs were prepared using two different BBR:polymer

ratios (1:5 and 1:10) with different volumes of GA (1.0 mL and 2.0 mL). Initially, an aqueous phase was prepared by adding a BBR solution (BBR in methanol) to an aqueous polymeric dispersion of Kollicoat® SR 30 D. After obtaining a clear solution, it was added to the light liquid paraffin (oil phase) and stirred at 600 rpm for approximately 30 min to form a stable water-in-oil emulsion. Then, 1.0 N sulfuric acid (H_2SO_4) and GA were added dropwise to the stable emulsion and stirred for 5–6 h., at 500 rpm to coacervate the phase and crosslink the MPs in a rigid manner. The MPs were further separated by vacuum filtration *via* successive washing with acetone to remove the oil residue, prevent the agglomeration of particles, and finally, washed with Milli-Q water. Finally, a 0.1 M glycine solution was used to wash the MPs to remove the untreated GA residues. The MPs were then dried at 40 °C for 24 h in a hot-air oven to obtain discrete well-formed particles. Blank MPs were prepared in a similar manner without the addition of BBR to the polymer dispersion.

Particle Size and Shape

The particle size of the MPs was measured using a static automated imaging technique (Morphologi G3, Malvern Panalytical, UK), with dry dispersion as the sampling method. Circular equivalent (CE) diameters of the prepared MPs were recorded. The size and shape of the MPs were visualized at 5.0 × magnification using the same technique, and the circularity value was determined accordingly.

Scanning Electron Microscopy (SEM)

The surface morphology of the crosslinked MPs was examined by field emission scanning electron microscopy (FESEM; JEOL JSM-7610F, UK). The MPs were coated with a platinum film using a sputter coater under an inert atmosphere and then fixed onto stubs using double-sided adhesive tape. The surfaces of the MPs were analyzed at a voltage of 15 kV, and FESEM images were captured at a suitable magnification.

% BBR Entrapment Efficiency

MPs in known quantities were crushed in a mortar and pestle and mixed with methanol. The above solution was sonicated for more than 6 h for complete extraction of BBR into the extraction solvent. The solution was centrifuged at 10,000 rpm for 30 min, and the supernatant was collected and analyzed using a UV-visible spectrophotometer (UV2600, Shimadzu, Japan) at a wavelength of 345 nm. The % BBR entrapment efficiency was calculated using the following formula:

$$\%\text{BBR entrapment efficiency} = \frac{\textit{Experimental BBR Content}}{\textit{Theoretical BBR Content}} \times 100 \quad (1)$$

Fourier Transform Infrared (FTIR) Spectra

FTIR spectra of pristine BBR, Kollicoat® SR 30 D, blank MPs, and BBR-loaded MPs were recorded to determine the chemical stability of BBR in the MPs and the crosslinking behavior of the polymer. The samples were scanned in the range of 4000–600 cm^{-1} using an FTIR instrument (Alpha II, Bruker, UK) in ATR mode.

Thermal Analysis

The thermal properties of pure BBR, Kollicoat® SR 30 D, blank MPs, and BBR-loaded MPs were evaluated by differential scanning calorimetry (DSC 3, Mettler Toledo, Switzerland). Approximately, 5.0 mg of each sample was weighed individually in an aluminum pan and sealed with a lid. DSC thermograms were obtained by heating the samples from 25 to 300 °C at a heating rate of 10 °C/min in a nitrogen (N_2) environment at a flow rate of 20 mL/min. For reference, an empty sealed aluminum pan was used.

Diffraction Studies

The molecular state (crystallinity) of pure and encapsulated BBR in the crosslinked MPs was investigated using X-ray diffraction (XRD) analysis. Powder XRD was performed using an X-ray diffractometer (Bruker D8 Advance, Germany), in which samples were scanned between an angle range of 5 and 70° at the 2θ plane using nickel-filtered Cu Kα radiation (λ = 1.5418 Å) at a voltage of 30 kV and a current of 15 mA. Three diffractograms were obtained, and the values were plotted using OriginPro® software.

Swelling Index

The swelling behavior of the crosslinked MPs was examined by determining the mean diameter of the MPs using laser diffraction analysis (Mastersizer 3000, Malvern, UK). The swelling behavior was studied in both acidic (pH 1.2) and alkaline (pH 6.8) media. The MPs were allowed to swell completely and reach equilibrium at 37 °C. After complete swelling, the swollen MPs were collected, and the mean volume diameter was determined. The % swelling was determined from the difference in MPs size before and after swelling and presented graphically.

In Vitro BBR Release

The *in vitro* release of BBR from the MPs was performed separately in acidic (pH 1.2) and alkaline (pH 6.8) media, representing both gastric and intestinal conditions, respectively. To determine the *in vitro* acid release behavior of BBR-MPs, they were filled in the previously prototyped in-house 3D printed capsules (size 00) (35) and were immersed in 200 mL of the acid dissolution medium and stirred at 100 rpm at 37 ± 1 °C. To determine the *in vitro* release behavior of BBR-MPs in intestinal medium (pH 6.8, phosphate buffer), the MPs were immersed directly under the same dissolution conditions as mentioned above. Aliquots were withdrawn at predetermined time intervals and replenished with an equal volume of a fresh dissolution medium. The collected aliquots were filtered through a 0.22-μm Millex syringe filter (Millipore Corporation) and analyzed spectrophotometrically at 345 nm.

Kinetics of BBR Release

The kinetics of BBR release from the MPs was determined after the *in vitro* BBR release study. The results from the *in vitro* BBR release study were fitted to several mathematical kinetic models (37–41), including the zero-order drug release model (Eq. 2), first-order drug release model (Eq. 3), Higuchi model (Eq. 4), Hixson-Crowell model (Eq. 5), and Korsmeyer-Peppas model (Eq. 6).

$$Q_t = Q_0 + K_0 t \tag{2}$$

$$logQ = logQ_0 - \frac{K_1 t}{2.303} \tag{3}$$

$$Q_t = K_H \times t^{12} \tag{4}$$

$$\sqrt[3]{Q_0} - \sqrt[3]{Q_t} = K_{HC} t \tag{5}$$

$$\frac{Q_t}{Q_\infty} = K_{KP} t^n \tag{6}$$

where Q_0, Q_t, and Q_∞ corresponds to the initial amount of drug at time zero, amount of drug released at time "t," and at infinite time, respectively. K_0, K_1, K_H, K_{HC}, and K_{KP} represent the release rate constants obtained from the zero-order, first-order, Higuchi, Hixson-Crowell, and Korsmeyer-Peppas release curves, respectively. "n" value in Korsmeyer-Peppas model is the release exponent which represents the release mechanism of the drug from the matrix.

In Vivo Pharmacokinetic Study

Oral pharmacokinetic studies of the optimized BBR-loaded MPs and pristine BBR were conducted in male New Zealand white rabbits (1–1.5 kg each). The study protocol was approved by the Institutional Animal Ethics Committee of the National Institute of Pharmaceutical Education and Research (Guwahati, India). Rabbits were kept in separate cages under 12-h light and dark cycles with proper air conditions in the room and provided a proper diet. Before the start of the experiment, the rabbits were fasted overnight and had access to only water. The rabbits were divided into two groups (three per group), where one group received pristine BBR and the other group received BBR-loaded MPs.

For the unit dosage administration of BBR and BBR-MPs *via* the oral route, a 3D printed hollow capsular device (size 03) was used, which was fabricated earlier in our lab and proved to release the drug within 30 min under GIT conditions *in vitro*. For administration to rabbits, the approximate size of the capsules (size 03) was printed into two parts (body and cap), as shown in Fig. S1. Both pristine BBR and BBR-MPs were filled in the 3D printed capsules at a unit dose of 5.0 mg and orally administered to rabbits with the help of a feeder.

Blood samples (0.5 mL) were collected from the marginal ear veins of the rabbits at predetermined time intervals. Blood samples were collected in EDTA-coated tubes (Microtainer, BD Labs) and gently upturned a few times to confirm the complete mixing of blood with the anticoagulant EDTA. Blood samples were centrifuged at 3500 rpm at 4 °C to separate the plasma from the blood cells. Plasma (supernatant) was collected and stored at −80 °C until further analysis.

UPLC-MS/MS Assay Validation

Preparation of Stock Solutions

The BBR stock solution was prepared by dissolving it in methanol (1.0 mg/mL). To prepare primary aliquots of BBR for the calibration curve and quality control (QC), serial dilutions were made using a stock solution of BBR. Similarly, a stock solution of 1.0 mg/mL, palmatine as IS was prepared in methanol, and a working solution of palmatine 50 ng/mL was prepared in methanol.

Preparation of Calibration and Quality Control (QC) Samples

Ten microliter of BBR primary aliquot was spiked in 90 μL of rabbit plasma to prepare calibration curve samples in a range of 0.75–500 ng/mL. Similarly, QC samples of BBR at low (2 ng/mL, LQC), middle (100 ng/mL, MQC), and high (200 ng/mL, HQC) concentrations in rabbit plasma, along with a lower limit of quantification (0.75 ng/mL, LLOQ), were prepared independently. All stock solutions of BBR were stored at 0–4 °C until further use.

Extraction of BBR from rabbit plasma

Plasma samples were collected from the defreezer and thawed at room temperature for 5 min in a water bath. The samples were then extracted using a simple protein precipitation method with a mixture of methanol and acetonitrile (1:1). To 90 μL of rabbit plasma (calibration standard and test sample), 1.0 mL of extraction solvent containing IS (50 ng/mL) was added. The mixture was then thoroughly mixed. The mixed solution was centrifuged at 8000 rpm at 4 °C, and the supernatant was collected. The supernatant was then evaporated using a vacuum concentrator. Methanol (100 μL) was used to reconstitute the sample.

UPLC-MS/MS Conditions

An Acquity UPLC instrument (Waters, MA, USA) was used for BBR analysis, which included a quaternary pump, a degasser, an auto sampler, and a column compartment. The Waters Xevo TQ-XS triple quadrupole system (Waters, MA, USA) with an electrospray ionization (ESI) source was used for mass spectrometric detection. Data acquisition and

instrument control were performed using the Mass Lynx software (Version 4.2). The analysis of BBR and IS from plasma samples was achieved using Water's BEH C18 column (150 mm × 2.1 mm I.D.; particle size 1.7 μm) and mobile phase composed of a mixture of (A) Water containing 0.1% formic acid and (B) acetonitrile containing 0.1% formic acid. BBR was eluted in the gradient program mode. The gradient for BBR elution was set as follows: (T_{min}/% proportion of solvent B): $_{0}$/5, $_{0–6}$/95, $_{6–6.5}$/95, $_{6.5–8}$/5, $_{8–10}$/5. The mobile phase flow rate was 0.3 mL/min, the column temperature was 45 °C, and the injection volume was 2 μL. The compound-dependent and instrumental parameters were optimized using neat BBR and IS solutions. The multiple monitoring mode (MRM) was used to quantify BBR in rabbit plasma. The MRM transitions for BBR and IS were *m/z* 336.00 > 278.00 and 352.00 > 320.00, respectively. A cone voltage of 6 V and collision energy of 38 eV were used for the BBR, and a cone voltage of 10 V and collision energy of 23 eV were used for the IS. The ESI inlet conditions, such as capillary voltage, cone voltage, source temperature, desolvation temperature, cone gas flow, and desolvation gas flow, used for the BBR analysis were 0.5, 3, 150, 500, 150, and 1000 L/h, respectively. The retention times of BBR and IS were 4.86 min and 4.82 min, respectively. Quantitative data analysis was performed using Target Lynx software. The developed method was validated according to the US FDA guidelines (42).

Pharmacokinetic Parameters

After the analysis of the plasma samples, a graph was plotted between the time and plasma concentration for both pristine BBR and BBR-loaded MPs. From the graph, the area under the plasma concentration-time curve (AUC) was determined using the linear trapezoidal method. Pharmacokinetic parameters included peak (maximum) plasma concentration (C_{max}), time required to achieve maximum plasma concentration (T_{max}), AUC from time zero to the last time point (AUC_{0-t}), AUC from time zero to infinity ($AUC_{0-\infty}$), and the elimination rate constant (K_{el}). The RBA was calculated from the AUC values of pristine BBR and BBR-MPs.

RESULTS AND DISCUSSIONS

Preparation of MPs

The poor oral bioavailability of BBR is contributed from both low solubility as well as extensive first pass metabolism and P-gp efflux. Due to this reason, high dose and frequent dosing is recommended for clinical use, and such high doses usually trigger adverse gastrointestinal reactions. So, a controlled drug delivery is an adoptive strategy to address these problems. Owing to poor oral bioavailability and high dose, sustained-release MPs of BBR were considered for the formulation. Sustained-release formulations will provide continuous release of BBR, maintaining a prolonged retention time inside the GIT, which promotes the continuous and constant availability of BBR in plasma. Additionally, the sustained-release formulation reduced the dose and dosing frequency. MPs are suitable for oral delivery of sustained-release formulations. Also, in the microparticles, the entrapped drug may present in amorphous form due to molecular dispersion of drug within the polymeric matrix, which may further supports in improving the solubility of drug in GIT. Although amorphous solid dispersion can certainly improve the solubility of drug, but here it was not feasible to formulate as the polymer used here is commercially available in liquid dispersion form, where we had successfully converted the mass from liquid to amorphous solid by emulsion crosslinking method. Polymer selection is crucial for the preparation of sustained-release MPs because the release behavior of BBR from MPs mainly depends on the physicochemical behavior of the polymer. Hence, to achieve sustained release, Kollicoat® SR 30 D, an aqueous dispersion of polyvinyl acetate stabilized with polyvinylpyrrolidone and sodium lauryl sulfate, was selected. Kollicoat® SR 30 D is widely used as a sustained-release coating polymer and matrix former in tablets and pellets (43–46). Sustained release is achieved through pH-independent swelling of this polymer in both stomach and intestinal regions (32). The preparation method used here was found to be suitable for the preparation of MPs because the polymer is available in liquid dispersion form. GA solution (25% v/v) was used to crosslink the polymers. Acid-catalyzed crosslinking of polyvinyl acetate in the presence of crosslinker GA is a spontaneous reaction that leads to the gelling of the polymer and further particle formation by continuous stirring for a specific period. Based on some preliminary trials, the minimum quantity of GA was fixed to 1.0 mL for crosslinking of the polymer. Below that quantity based on the total weight of the drug:polymer taken, it was observed low crosslinking intensity of the emulsion template followed by the formation of non-rigidized softened microparticles, whereas on higher than this 2.0 ml of quantity, there might be a serious concern of toxicity due to unreacted GA which will further demand for successive multiple times washing with 0.1 N glycine to remove the same (36). Therefore, for a better suited comparative study, the maximum quantity of GA was restricted to 2.0 mL (keeping in mind the maximum allowed concentration) where effect of GA can be analyzed at two level, *i.e.*, lower and higher. The addition of BBR to the polymeric mixture before crosslinking results in the formation of a BBR-loaded polymeric matrix. Four batches of BBR-loaded MPs (Table I) were prepared with varying BBR:polymer ratios and GA solution volumes. The crosslinked MPs were yellowish in color owing to the BBR color characteristics.

Particle Size and Shape

The particle size remained almost constant irrespective of the BBR:polymer ratio or GA concentration. The particle sizes of all batches of MPs are listed in Table II, and particles size distribution graphs are shown in Fig. 1. Usually, the stirring speed used during the fabrication of MPs provides a shearing force that causes the breakdown of the emulsion or crosslinked matrix into smaller droplets that form BBR-loaded MPs after drying. As a constant stirring speed was maintained for all batches of MPs, no significant difference in particle size was observed despite varying the BBR:polymer ratio and crosslinker concentration. In addition, the viscosity of the dispersed phase was equivalent for both BBR:polymer ratios; as a result, no effect of polymer concentration on particle size was observed. It was also reported that on increasing the concentration of GA, there was no significant change in the size of MPs observed (47). A similar observation was made in this study, where all batches of MPs had almost equivalent particle sizes.

Table I Formulation Code of Different Batches of MPs

Formulation	Drug:polymer ratio	GA (mL)
F1	1: 5	1
F2	1: 5	2
F3	1: 10	1
F4	1: 10	2

Particles Surface Morphology

Before drying, digital images were obtained (Fig. S2), and the MPs were both spherical and smooth. During drying, these crosslinked MPs underwent shrinkage and water loss, resulting in the formation of spherical and distorted particles. The spherical nature of MPs was observed using static automated imaging (Fig. 2) and SEM (Fig. 3). The size and shape of the MPs also depend on the dispersion medium in which the light liquid paraffin was found to be suitable, which is also supported by other studies. All batches of MPs had a circularity value near 1 (Table II), which indicated the circular structure/spherical structure of the particles. The MPs also possessed a smooth surface without any debris/residue, as confirmed from the SEM micrographs (Fig. 3), which indicated that BBR was dispersed in the MPs because no drug crystals were traced.

% BBR Entrapment Efficiency

The entrapment efficiency of BBR inside crosslinked MPs was determined using UV-visible spectroscopy, and the results are presented in Table II. % BBR entrapment efficiency was affected by the BBR:polymer ratio and GA concentration. BBR entrapment was found to be maximum at a lower concentration of GA, whereas at higher concentrations of GA, drug entrapment declined irrespective of the BBR:polymer ratio. MPs with a BBR:polymer ratio of 1:10 and a lower volume of GA solution (F3) yielded the highest % BBR entrapment efficiency of approximately 81.63% ± 4.9. It can be observed that the entrapment efficiency of BBR in MPs increased with increasing polymer concentration; however, in batch F4, the entrapment efficiency did not increase as expected, which might be due to the high concentration of the crosslinker. A higher concentration of the crosslinker might decrease the entrapment behavior of BBR during crosslinking of the polymer. A similar phenomenon was observed by Ofokansi et al. (48). Hence, this type of similar effect was observed for both BBR:polymer ratios.

Thermal Analysis

To investigate the solid-state properties of BBR after encapsulation inside the MPs, DSC was performed for pristine BBR, Kollicoat® SR 30 D, blank MPs, and BBR-loaded MPs from 25 to 300 °C. The thermograms obtained are shown in Fig. 4. BBR showed a sharp endothermic peak at 191 °C (the melting point of BBR), which is similar to the literature (49). The Kollicoat® SR 30 D was stable over the tested range. In the case of BBR-loaded MPs, the melting endothermic peak of BBR was absent, indicating molecular dispersion of BBR in the crosslinked polymeric matrix of Kollicoat® SR 30 D. This confirmed the conversion of the crystalline form of BBR to an amorphous state after the formation of MPs. However, crystallinity was further confirmed by powder XRD analysis.

Diffraction Studies

XRD is an efficient analytical technique to confirm the crystallinity of BBR and polymers. The XRD diffractograms of BBR, blank MPs, and BBR-loaded MPs are shown in Fig. 5 The crystalline nature of pristine BBR was confirmed by the appearance of sharp characteristic peaks at different diffraction angles (at the 2θ plane) of 6.67°, 8.64°, 9.12°, 13.00°, 16.32°, 24.54°, and 25.56°. However, these crystalline peaks were not observed for the BBR-loaded MPs, confirming the amorphous nature of BBR in the polymeric crosslinked MPs. As shown in Fig. 5, both blank MPs and BBR-loaded MPs had almost identical diffractograms with broad peaks and less intense peaks, indicating no undesirable interactions between BBR and the polymer, and a loss of crystallinity was attained.

FTIR Spectra

To examine the chemical interaction between BBR and the polymer and to confirm the crosslinking of the polymeric matrix, FTIR analysis was conducted for pristine BBR, Kollicoat® SR 30 D, blank MPs, and BBR-loaded MPs in ATR mode. The FTIR spectra of all samples are shown in Fig. 6. All the characteristic peaks of the samples were observed in their respective spectra. Pristine BBR showed intense transmittance at 3316, 3052, 2944, 2842, 2769, 1601, 1642 1500, 1331, 1268, 1221, 1102, 1031, 904, and 827 cm^{-1}, which are characteristic peaks reported in the literature (50). The peaks at 2842 and 1642 cm^{-1} corresponds to the methoxy group and C=N double bond, respectively. In addition, the signal at 1500–1600 cm^{-1} represents aromatic C-H bending (26). As the polymer present in dispersion form, the FTIR spectra of Kollicoat® SR 30 D had shown broad peak at 3354 cm^{-1} due to water, followed by peaks at 1713, 1641, 1428, 1376, 1261, and 1027 cm^{-1}. The blank MPs exhibited characteristic peaks at 3931, 3760, 3676, 3427, 3345, 3190, 1858, 1729, 1663, 1507, 1421, 1365, 1235, 1127, 1011, and 937 cm^{-1}, which correspond to polymer peaks as well as some other characteristic peaks that correspond to the crosslinking of the polymer, such as the peak at 1127 cm^{-1}, representing the formation of acetal bonds due to crosslinking of the polymer in the presence of GA. Similarly, the BBR-loaded MPs showed almost the same band as blank MPs and BBR with reduced intensities and without any major shift in peak position,

Table II Particles Size, Circularity, and Entrapment Efficiency of MPs

Formulation	Particles size, D [*n*, 0.5] (μm)	Circularity	Entrapment efficiency (%)
F1	11.62	0.964	71.16 ± 5.4
F2	11.09	0.976	60.37 ± 4.5
F3	11.31	0.961	81.63 ± 4.9
F4	11.18	0.971	54.38 ± 5.5

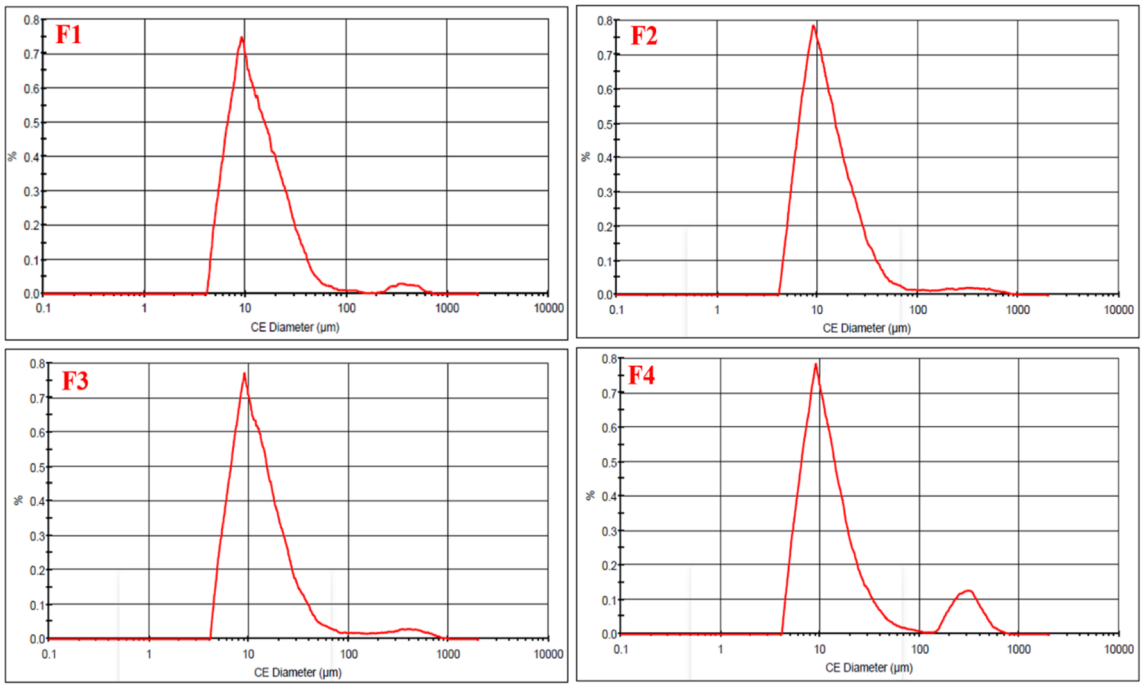

Fig. 1 Particles size distribution of all batches of microparticles

indicating that there was no unfavorable chemical interaction between the BBR and polymer during the preparation of the MPs, confirming the stability of BBR in MPs.

Swelling Index

Since Kollicoat® SR 30 D is a pH-independent polymer, the release of the drug mainly depends on the swelling of the matrix. Therefore, the swelling index is a crucial parameter for crosslinked MPs and directly influences the BBR release profile. A swelling study was conducted to determine the changes in the volume diameter of the swollen particles. Particle volume diameters were determined using a particle size analyzer. The results of the swelling study are shown in Fig. 7. The graph indicates that with increasing concentration of crosslinker, swelling of the MPs decreased, and this effect was observed with both drug:polymer ratios. The reduction in swelling with a higher crosslinker concentration is due to the formation of a rigid network structure and lower water uptake. At lower crosslinker concentrations, a loose network is formed; hence, the particles have a high hydrodynamic free volume to detain more water molecules (51). With an increase in the drug:polymer ratio, an increase in the swelling index value was observed, where both the F3 and F4 batches

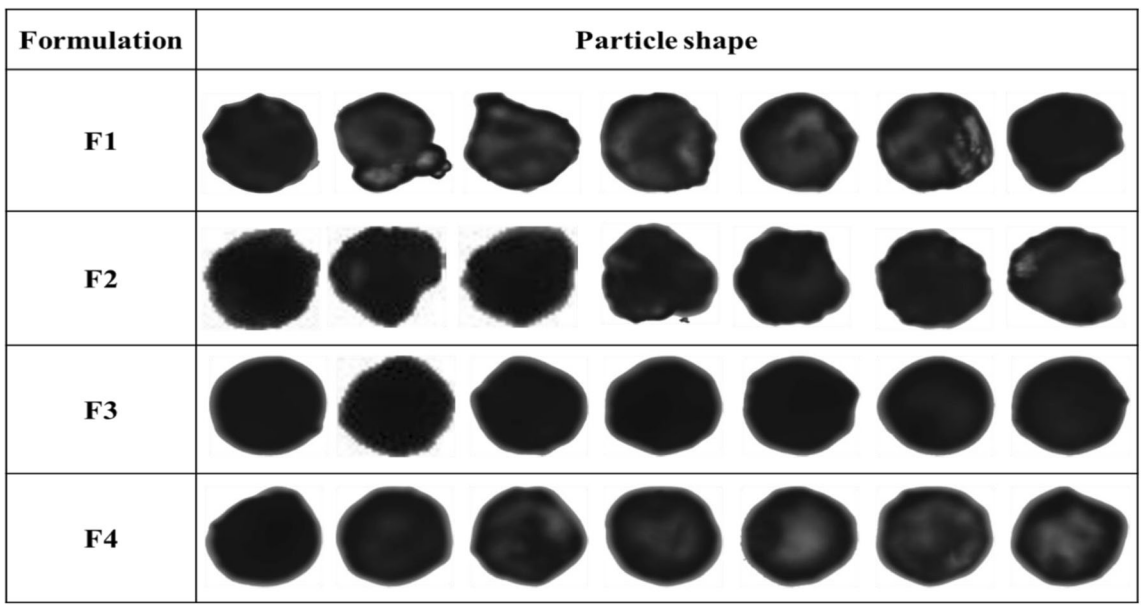

Fig. 2 Particles shape analysis by static automated imaging technique

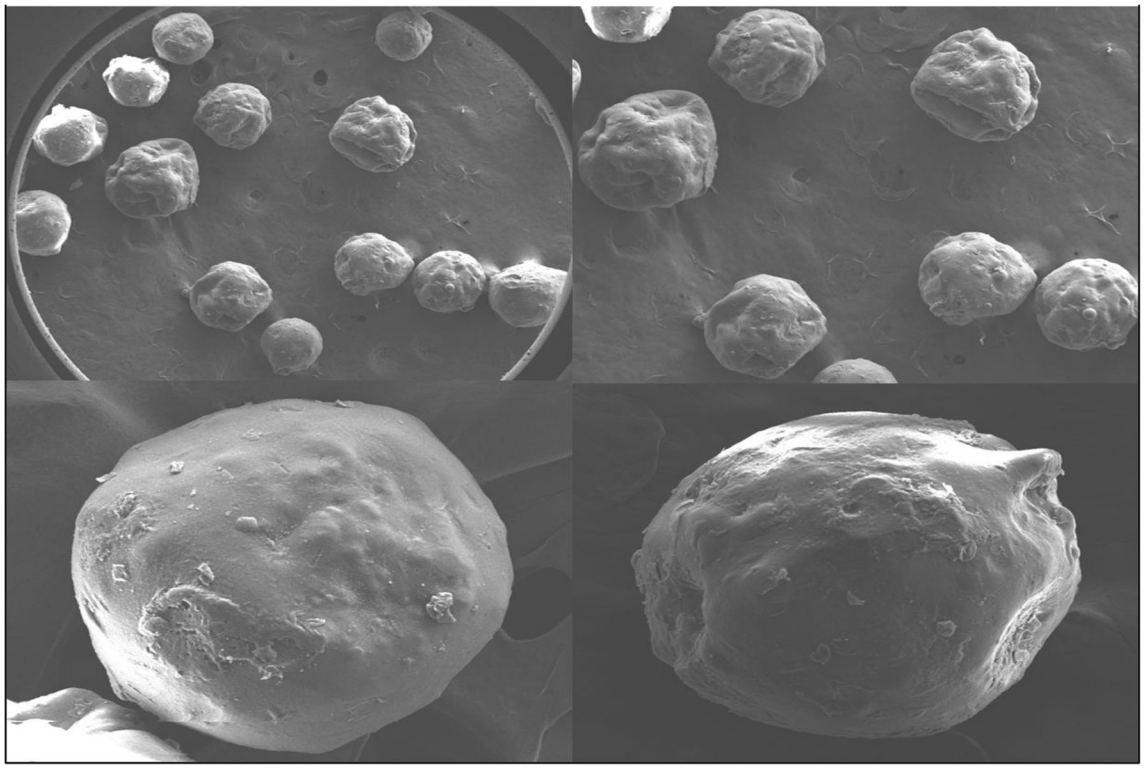

Fig. 3 Scanning electron micrographs of BBR-loaded MPs showing the spherical nature with smooth surface

(higher drug:polymer ratio) showed more swelling than the F1 and F2 batches (lower drug:polymer ratio). Overall, F3 batch showed highest swelling index value due to combined effect of higher drug:polymer ratio and lower crosslinker concentration. Additionally, swelling of the particles was slightly higher in the alkaline medium. Among the four batches of MPs, the F3 batch showed the highest swelling in both acidic and alkaline media (74.43% ± 7.04 and 84.96% ± 4.39, respectively). The results of the swelling study were observed in the *in vitro* BBR release profiles of the MPs.

In Vitro BBR Release and Kinetics

The *in vitro* release of BBR from the MPs was conducted in both acidic and alkaline media, representing gastric and intestinal conditions, respectively. The cumulative BBR percentage release with respect to time for all four batches of MPs under both acidic and alkaline pH conditions is shown in Figs. 8 and 9, respectively. BBR-loaded MPs showed sustained release in both acidic and alkaline media because of the pH-independent swelling behavior of the polymer. For BBR release in an acidic medium, BBR-MPs were filled in an

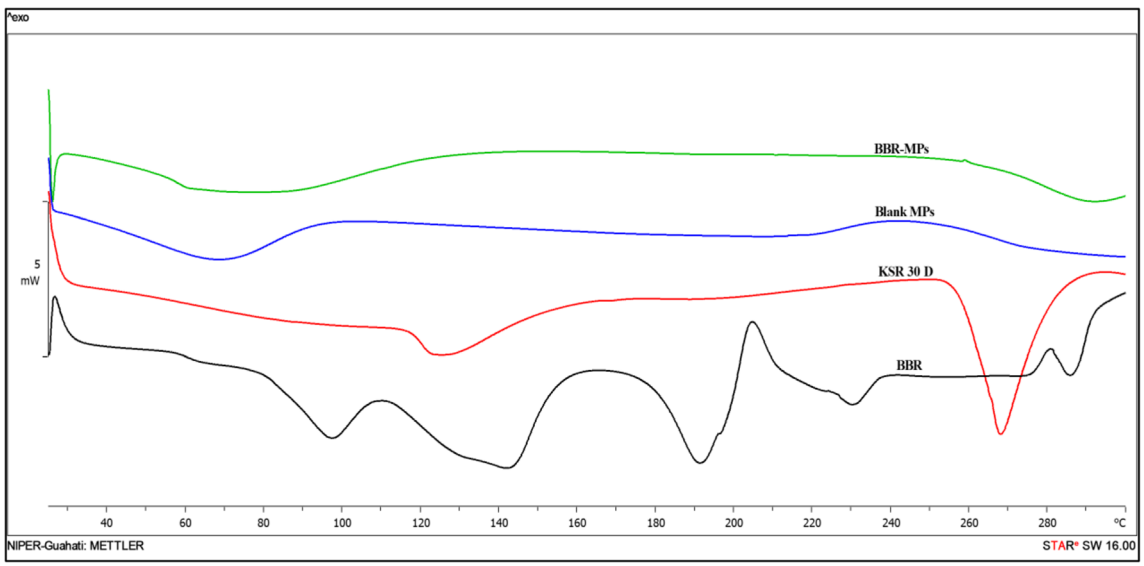

Fig. 4 DSC overlay of pristine BBR, Kollicoat® SR 30 D, blank MPs, and BBR-loaded MPs

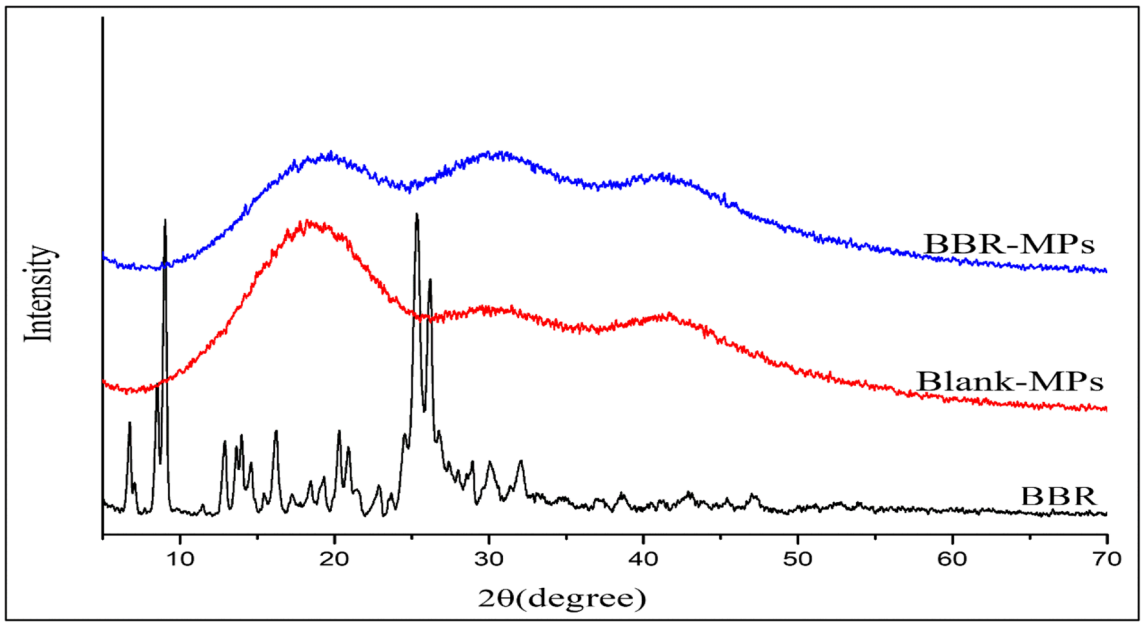

Fig. 5 XRD overlay of pristine BBR, blank MPs, and BBR-loaded MPs

in-house fabricated 3D printed capsular device, and the release study was conducted. As per our earlier reports (35), the capsular device starts erode within 10–15 min, and the encapsulated BBR-MPs do not come into contact with the dissolution medium early. Hence, no BBR was released for up to 15 min. After 30 min, BBR was detected in the dissolution medium as the capsule burst (Fig. S3), and the encapsulated MPs encountered the dissolution medium. The F1, F2, and F4 batches showed BBR release up to 4.39% ± 0.106, 3.84% ± 0.302, and 5.37% ± 1.025, respectively, within 4.0 h. (maximum gastric emptying time), whereas the F3 batch showed a BBR release of 10.64% ± 1.131 (Fig. 8). The release of BBR from MPs in an alkaline medium was conducted separately (Fig. 9). In this case, BBR-MPs were directly added to the dissolution medium as the 3D printed hollow capsular device was completely eroded in acidic medium. The release of BBR was better in alkaline media than in acidic media. In the alkaline medium, BBR release was conducted for 72 h, and all batches showed more than 40% BBR release. The F1, F2, and F4 batches showed BBR releases of 46.31% ± 5.93, 43.08% ± 4.48, and 40.91% ± 1.81, respectively, whereas the F3 batch showed 75.13% ± 2.24 BBR release.

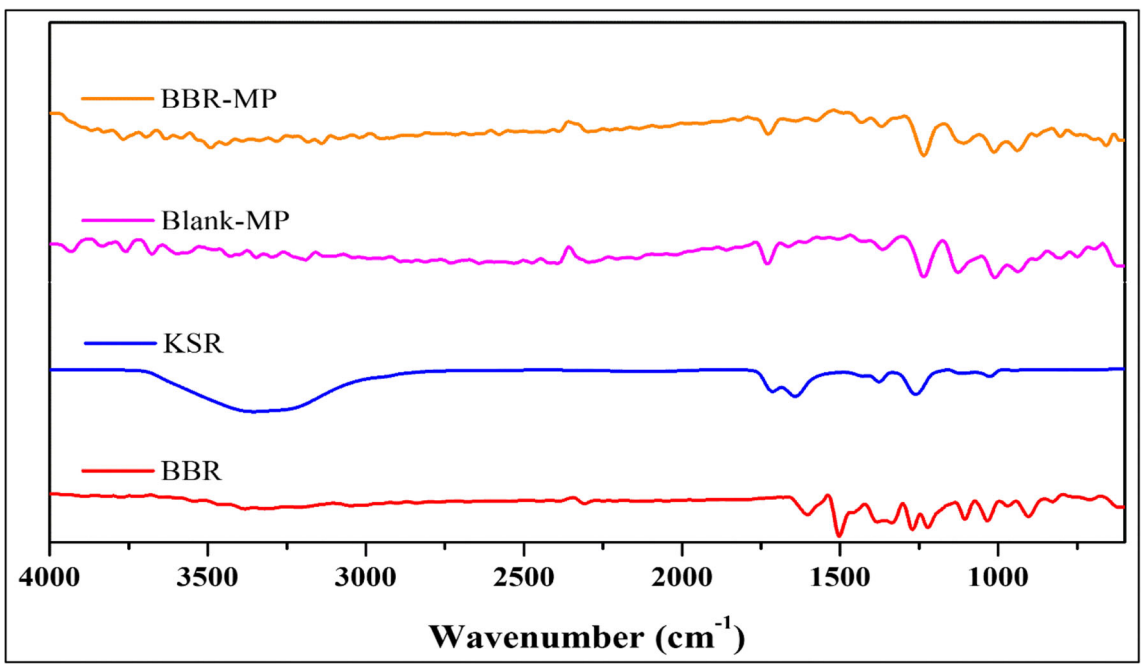

Fig. 6 FTIR spectral overlay of pristine BBR, Kollicoat® SR 30 D, blank MPs, and BBR-loaded MPs

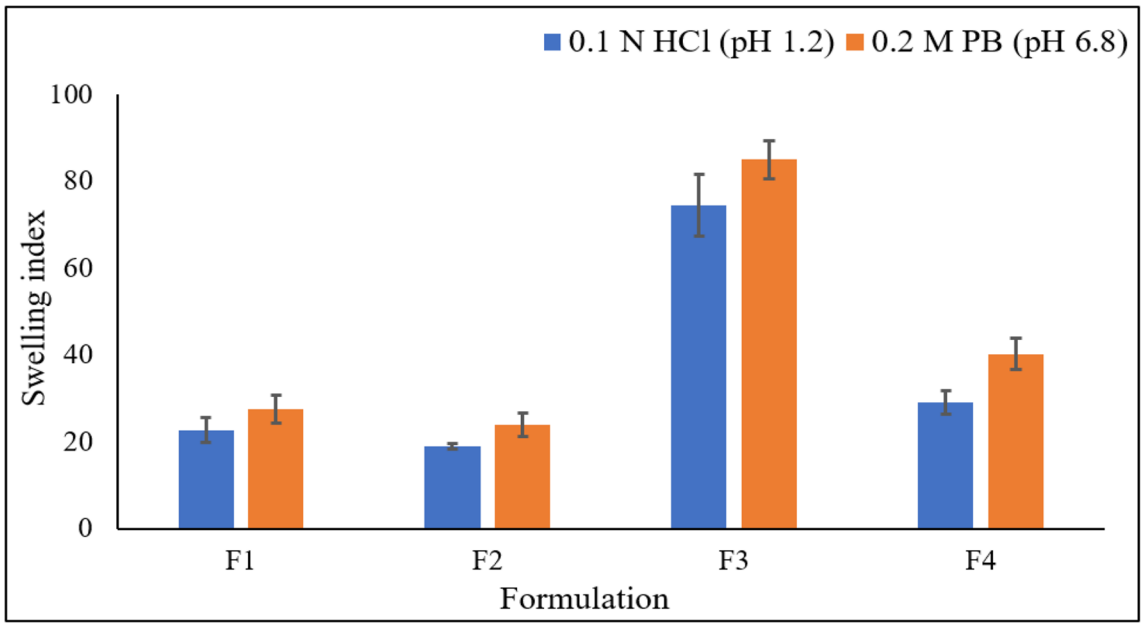

Fig. 7 Swelling index behavior of BBR-MPs in both acidic and alkaline medium

From the *in vitro* BBR release profile, it was observed that the release of BBR from the MPs was characterized by a slow-release profile, which implied a sustained release efficiency of the crosslinked MPs. MPs prepared with a higher concentration of crosslinker had the slowest release rate of BBR compared to the MPs prepared with a lower concentration of crosslinker. This might be explained by the assumption that, with a higher concentration of crosslinker, denser particles were formed, which prevented the diffusion of entrapped BBR into the dissolution medium, and the swelling of these MPs was restricted. Similar observations were also reported, where with a lower concentration of crosslinker, the degree of crosslinking of the polymer decreases as the polymer network density decreases. In this case, BBR diffusion from the polymeric matrix increased, which was supported by the enhanced swelling. Conversely, on increasing the concentration of the crosslinker, the polymer crosslinking density increased and the BBR diffusion process was reduced, resulting in a decrease in the BBR release rate (51, 52). A significant increase in drug release was found with increased drug:polymer ratio but was limited to the F3 batch only where the concentration of crosslinker was low. In F4 batch, BBR release was not increased significantly despite of higher drug:polymer ratio which might be due to presence of higher concentration of crosslinker that leads to slower drug release. It was also observed that BBR-

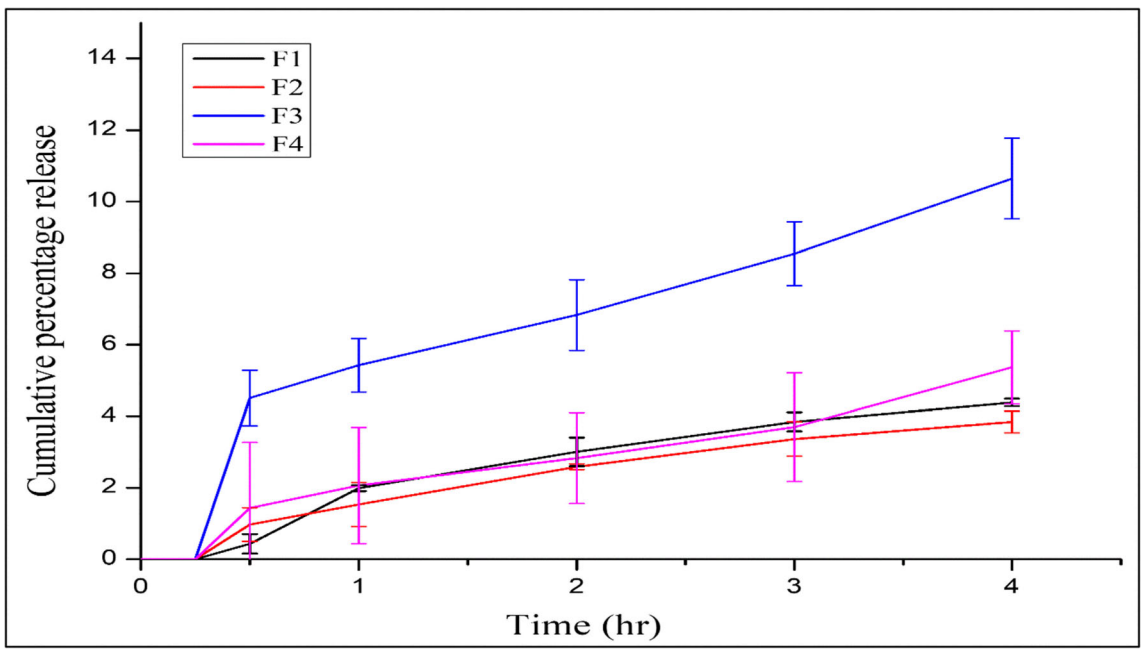

Fig. 8 *In vitro* BBR release profile from prepared MPs in 0.1 N HCl, pH 1.2

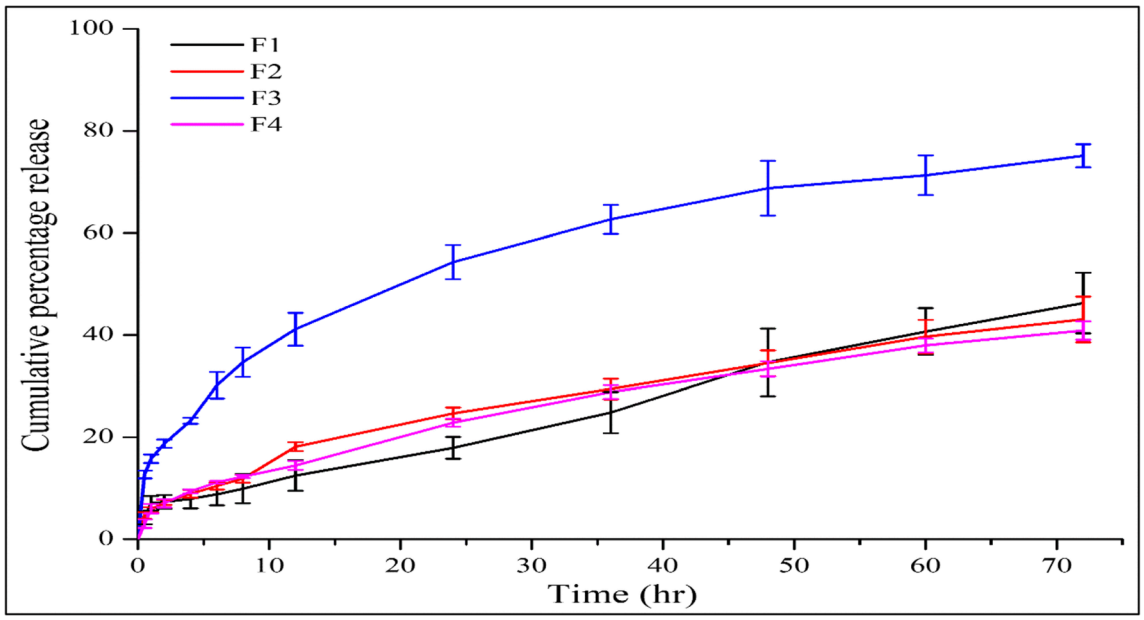

Fig. 9 *In vitro* BBR release profile from prepared MPs in 0.2 M phosphate buffer, pH 6.8

loaded MPs showed better release in alkaline medium than in acidic medium. This behavior was observed because of the increased swelling of the crosslinked polymeric matrix in the alkaline medium. As a result, more BBR was released in the alkaline medium. The release behavior in both media was also supported by the swelling study observed in both acidic and alkaline media, where the swelling index of MPs in an alkaline medium was greater than that in an acidic medium.

Sustained release behavior of the drug for a prolong period may tends to recrystallization of the drug in dissolution media. Hence, by determining the XRD of BBR in dissolution media might give an insight to the solubility and dissolution behavior of the same for a longer period of time. But, in this case, it is not feasible to determine the XRD of BBR from the dissolution test as end solid comprised of BBR with used polymeric matrix which makes very difficult to isolate BBR as final end solid to accurately determine its XRD behavior.

Mathematical kinetic models were used for parametric depiction of the *in vitro* BBR release data. The results of the *in vitro* release study were fitted to different mathematical release kinetic models and the best-fit model was selected based on the highest determination coefficient value. From the correlation coefficient values of all release kinetics models shown in Table III, a high correlation was observed for the Korsmeyer-Peppas model in both acidic and alkaline media. From the Korsmeyer-Peppas model, the "n" value was calculated for all batches of MPs, which provides insight into the mechanism of BBR release. The *n* values for all batches of MPs in the acidic and alkaline media were greater than 0.5, as presented in Table III. As the "n value" lies between 0.5 and 1, it indicates the anomalous transport where the release of BBR from the MPs was governed by swelling of the polymeric matrix followed by diffusion of BBR.

The stability testing study of MPs was not analyzed further as several studies were already been well reported on the stability profile of MPs over 3 to 12 months, where MPs were found to be stable throughout the tested period (24, 53–56). Moreover, we explored detailed *in vitro* physicochemical investigations with emphasis on solid-state analysis through DSC and XRD studies in order to ensure its solid-state potential.

Table III Correlation Coefficient (R^2), *k* and *n* Values from Various BBR Release Models from the MPs ($n = 3$)

Formulation		Zero order		First order		Higuchi		Korsmeyer-Peppas			Hixson-Crowell	
		r^2	K_0	r^2	K_1	r^2	K_H	r^2	K_{KP}	n	r^2	K_{HC}
F1	HCI	0.8766	1.233	0.8836	0.013	0.8785	2.093	0.9446	1.688	0.772	0.8813	0.004
	PB	0.9278	0.688	0.9475	0.009	0.9474	4.807	0.9745	2.517	0.673	0.9429	0.003
F2	HCI	0.8589	1.080	0.8673	0.011	0.9552	1.848	0.9944	1.597	0.651	0.8646	0.004
	PB	0.8277	0.698	0.8919	0.009	0.9945	5.006	0.9955	4.576	0.524	0.8730	0.003
F3	HCI	0.2684	2.960	0.3254	0.031	0.9466	5.178	0.9579	5.460	0.543	0.3067	0.010
	PB	1.335	0.4853	0.8028	0.030	0.9496	9.949	0.9944	15.797	0.573	0.7216	0.008
F4	HCI	0.8684	1.356	0.8739	0.014	0.9003	2.307	0.9522	1.914	0.692	0.8721	0.005
	PB	0.8317	0.666	0.8920	0.009	0.9959	4.779	0.9969	4.349	0.525	0.8742	0.003

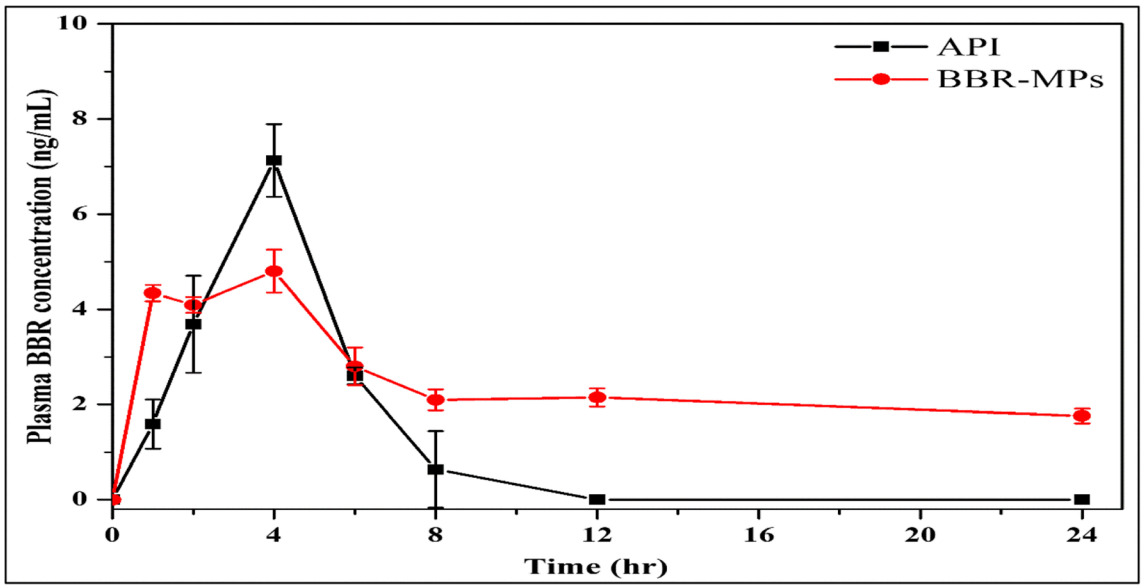

Fig. 10 Mean plasma concentration *Vs.* time profiles for BBR after oral administration of pristine BBR and BBR-loaded MPs filled in 3D printed hollow capsules at 5 mg kg^{-1} in rabbits ($n = 3$)

In total, four batches of BBR-MPs were prepared using two variables, *i.e.*, drug:polymer ratio and GA concentration. Among these four batches, F3 batch (higher drug:polymer ratio and lower concentration of GA) found to have promising *in vitro* physicochemical performances compared to other. This might be due to the increase in polymer ratio that can accommodate more quantity of BBR at low GA volume for better crosslinking with no shrinkage of the developed polymeric matrix.

In Vivo Pharmacokinetic Study

The extravascular non-compartmental method was used for pharmacokinetic analysis. The oral pharmacokinetic parameters of BBR were systematically compared after oral administration of both pristine BBR and BBR-loaded MPs (F3 batch) filled in in-house 3D printed hollow capsular device. The plasma concentration-time curve is presented in Fig. 10, where both pristine BBR and BBR-MPs were orally administered at a single dose of 5.0 mg. The capsule size that was used *in vivo* study can accommodate the maximum amount of BBR-MPs which is equivalent to 5.0 mg of pure BBR. As only pharmacokinetic profile of pure BBR to the formulated BBR was compared, there is no limitation in the use of specific amount of the same. Hence, 5.0 mg was used as a unit oral dose for conducting *in vivo* pharmacokinetic study in rabbits. The pharmacokinetic parameters obtained from the plasma concentration-time plots are summarized in Table IV. The plasma concentration-time curve for BBR-MPs displayed two peaks rather than a single peak curve, as observed for pristine BBR, which may be due to the sustained release of BBR from the MPs. A similar effect was observed by Jia et al., who prepared BBR-loaded solid proliposomes to enhance bioavailability (57). With the swelling of MPs, the continuous sustained release of BBR into the GIT environment results in a continual plasma concentration over time. After 8.0 h of oral administration, BBR was barely detected in the case of pristine BBR, whereas for BBR-MPs, BBR was detected up to 24 h with a plasma concentration of 1.76 ± 0.15 ng/mL. The C_{max} value for pristine BBR (7.131 ± 0.76 ng/mL) was found to be higher than that of BBR-MPs (4.803 ± 0.45 ng/mL), which is obvious for BBR-MPs as it is a sustained release formulation, and the availability of BBR at early time points was minimal. Similar trend of low C_{max} was also observed in various literature where at a dose of 100 mg/kg of BBR in rats showed C_{max} value in between 3.9 and 15 ng/mL (58–60). In both cases, T_{max} was 4 h. In addition, with other pharmacokinetic parameters, BBR-MPs showed better performance than pristine BBR, and the values are listed in Table IV. The RBA was calculated from the AUC values of pristine BBR and BBR-MPs, and it was found that the RBA of BBR-MPs was 2.19 times higher than that of the pristine BBR. These results indicate that the fabrication of pH-independent sustained-release MPs of BBR is effective in enhancing oral bioavailability by modulating their release in the GIT. In addition, sustained-release MPs can be used as an effective approach to improve the RBAs of BBRs with a high first-pass effect and P-gp efflux.

Table IV Pharmacokinetic Parameters for BBR After Oral Administration of Pristine BBR and BBR-Loaded MPs to Rabbits at a Dose of 5 mg kg^{-1} ($n = 3$)

Parameters	Pristine BBR	BBR-MPs
C_{max} (ng/mL)	7.131 ± 0.76	4.803 ± 0.452
T_{max} (h)	4	4
$AUC_{0\text{-}t}$ (ng/mL*h)	27.299 ± 3.270	59.758 ± 0.497
$AUC_{0\text{-}\infty}$ (ng/mL*h)	28.699 ± 5.400	99.911 ± 9.090
K_{el} (h^{-1})	0.205 ± 0.098	0.042 ± 0.006
$t_{1/2}$ (h)	4.29 ± 2.83	16.513 ± 2.322
Relative bioavailability	1	2.19

Table V Validation Parameters of the Used Bioanalytical Method

	LLOQ	LQC	MQC	HQC
Intra-day precision and accuracy				
Theoretical concentration (ng/mL)	0.75	2.5	100	200
Mean estimated concentration (ng/mL) ± SD	0.65 ± 0.07	2.72 ± 0.15	101.93 ± 1.29	198.29 ± 1
Precision (RSD, %)	11.75	5.65	2.5	0.81
Accuracy (%)	87.33 ± 10.26	87.33 ± 10.26	108.85 ± 6.54	99.14 ± 0.80
Inter-day precision and accuracy				
Theoretical concentration (ng/mL)	0.75	2.5	100	200
Mean estimated concentration (ng/mL) ± SD	0.61 ± 0.04	2.60 ± 0.09	104 ± 15 ± 3.80	202.59 ± 7.36
Precision (RSD, %)	7.15	3.81	3.65	3.63
Accuracy (%)	81.88 ± 5.85	104.28 ± 3.97	104.15 ± 3.80	101.29 ± 3.68

UPLC-MS/MS Assay Validation

The developed method was validated for the determination of BBR in rabbit plasma. The specificity of the BBR method was investigated by screening blank rabbit plasma for interference. No interference was observed at the retention times of the BBR and IS. The carryover effects of BBR and IS were tested, and no carryover was observed. The method was linear over a calibration range of 0.75–500 ng/mL for BBR in rat plasma. The calibration curve showed linearity with a mean correlation coefficient (r^2) of 0.999 for BBR. The limit of detection for BBR was 0.5 ng/mL. The lower limit of quantification (LLOQ) for BBR was 0.75 ng/mL. The intra- and inter-batch precision and accuracy of the developed method were studied by analyzing QC samples at three distinct concentrations for three replicates, including the LLOQ. The percent RSD was used to assess the precision of the method, whereas the percent recovery was used to assess its accuracy. Detailed information is presented in Table V. The intra- and inter-day precision of BBR for all QCs ranged from 0.81 to 11.75% and 3.63 to 7.15%, respectively. The intra- and inter-day accuracies for BBR for all the QCs ranged from 87.33 to 108.85% and 81.88 to 101.29%, respectively. The accuracy and precision of the method were within acceptable ranges. The matrix effect was assessed using three QC samples with different concentrations in six replicates. Matrix effects were not observed. The extraction recovery of BBR from the rabbit plasma samples was determined at three different levels (LQC, MQC, and HQC). The recoveries were within the acceptable range, and the mean recovery ranged from 89.55 to 97.23%.

CONCLUSIONS

Owing to the poor oral bioavailability and short half-life of BBR, pH-independent sustained-release MPs have been developed using emulsion crosslinking. The sustained release of BBR from the polymeric matrix will enable the continuous availability of BBR in the GIT for absorption, which will reduce the high dose and dosing frequency. It can be concluded that Kollicoat® SR 30 D-mediated MPs can be effectively prepared using the emulsion crosslinking method and the MPs displayed the desired sustained release behavior of BBR. As the BBR release profile from the MPs greatly depends on the crosslinking density, this MPs preparation method provides a suitable platform for controlling the release of BBR with any specific release rate by varying the crosslinking density of the MPs. In BBR-loaded MPs, BBR is primarily converted to an amorphous form as it is molecularly dispersed in the polymeric matrix; hence, amorphization of BBR leads to enhanced solubility in the GIT fluid. Seeing the emergence of cutting-edge next generation future green technology, *i.e.*, additive manufacturing-AM/3DP technology, for the unit dose delivery of the microparticles, an in-house 3D printed capsule was designed, customized, and used instead of simple capsule to make the dosage form more precise, personalized, and highly tailored made based on individual need. This kind of dosage form also provides more design and delivery flexibility in terms of individual preference that can only be achieved through this emergence AM technology rather conventional one. 3D printed capsules can be printed at the time of requirement, which will address the issue of shelf life of conventionally manufactured products, along with more flexibility in terms of size and shape. Therefore, we intended to coupled particulate technology (microparticles) with this newly evolving AM technology for pharmaceutical application which is yet to be explored for satisfying the needs of personalized medicines.

SUPPLEMENTARY INFORMATION

The online version contains supplementary material available at https://doi.org/10.1208/s12249-022-02241-9.

ACKNOWLEDGMENTS

The author sincerely acknowledges the financial support received from DPRP, DST, Ministry of Science and Technology, Government of India, through a National Facility (State-of-the-art infrastructure) project entitled “Establishment of a National Centre of Pharmacoengineering for designing innovative delivery strategies to fight neglected diseases” vide File No: VI-D&P/646/2018-19/TDT.

We would also like to acknowledge the North East Centre for Biological Sciences and Healthcare Engineering (NECBH), IIT Guwahati, and Department of Biotechnology (DBT), Govt. of India, for Project No. BT/COE/34/SP28408/2018 for the XRD and FESEM instrumentation facilities.

AUTHOR CONTRIBUTIONS

DC and AJ: data curation, formal analysis, investigation, methodology, validation, visualization, and writing—original draft. USN: project administration, resources, and funding acquisition. SB and RMB: conceptualization, formal analysis, funding acquisition, investigation, methodology, resources, supervision, validation, visualization, writing, review, and editing.

FUNDING

This work is funded through a National Facility (State-of-the-art infrastructure) project entitled "Establishment of a National Centre of Pharmacoengineering for designing innovative delivery strategies to fight neglected diseases" vide File No: VI-D&P/646/2018-19/TDT by the Drugs and Pharmaceuticals Research Programme (DPRP), Department of Science & Technology (DST), Ministry of Science and Technology, Government of India.

DECLARATIONS

Conflict of Interest The authors declare no competing interests.

REFERENCES

1. Neag MA, Mocan A, Echeverría J, Pop RM, Bocsan CI, Crisan G, et al. Berberine: Botanical Occurrence, traditional uses, extraction methods, and relevance in cardiovascular, metabolic, hepatic, and renal disorders. Front Pharmacol. 2018.
2. Sharma M, Satyavati G V, Raina MK, editors. Medicinal plants of India / [editors, G. V. Satyavati, M. K. Raina, M. Sharma]. New Delhi: Indian Council of Medical Research; 1976.
3. Imenshahidi M, Hosseinzadeh H. Berberine and barberry (*Berberis vulgaris*): a clinical review. Phyther Res [Internet]. John Wiley & Sons, Ltd; 2019 [cited 2021 Nov 10];33:504–23. Available from: 10.1002/ptr.6252.
4. Kumar A, Ekavali, Chopra K, Mukherjee M, Pottabathini R, Dhull DK. Current knowledge and pharmacological profile of berberine: an update. Eur J Pharmacol. Elsevier; 2015;761:288–297.
5. Swabb EA, Tai YH, Jordan L. Reversal of cholera toxin-induced secretion in rat ileum by luminal berberine. Am J Physiol [Internet]. Am J Physiol; 1981 [cited 2021 Nov 10];241:248–52. Available from: https://pubmed.ncbi.nlm.nih.gov/7282933/
6. Cernakova M, Košťálová D. Antimicrobial activity of berberine—a constituent ofMahonia aquifolium. Folia Microbiol 2002 474 [Internet]. Springer; 2008 [cited 2021 Nov 10];47:375–8. Available from: 10.1007/BF02818693
7. Vuddanda PR, Chakraborty S, Singh S. Berberine: a potential phytochemical with multispectrum therapeutic activities. https://doi.org/101517/135437842010517745 [Internet]. Taylor & Francis; 2010 [cited 2021 Nov 10];19:1297–307. Available from: 10.1517/13543784.2010.517745
8. Chen XW, Di YM, Zhang J, Zhou ZW, Li CG, Zhou SF. Interaction of herbal compounds with biological targets: a case study with berberine. Sci World J [Internet]. Hindawi Limited; 2012 [cited 2021 Nov 10];2012. Available from: /pmc/articles/PMC3504405/.
9. Warowicka A, Nawrot R, Goździcka-Józefiak A. Antiviral activity of berberine. Arch Virol [Internet]. Springer; 2020 [cited 2021 Nov 10];165:1935–45. Available from: 10.1007/s00705-020-04706-3
10. Varghese FS, Thaa B, Amrun SN, Simarmata D, Rausalu K, Nyman TA, et al. The antiviral alkaloid berberine reduces chikungunya virus-induced mitogen-activated protein kinase signaling. J Virol [Internet]. American Society for Microbiology; 2016 [cited 2021 Nov 24];90:9743–57. Available from: 10.1128/JVI.01382-16.
11. De Sarkar S, Sarkar D, Sarkar A, Dighal A, Staniek K, Gille L, et al. Berberine chloride mediates its antileishmanial activity by inhibiting Leishmania mitochondria. Parasitol Res. 2019.
12. Li Z, Garner AL, Gloeckner C, Janda KD, Carlow CK. Targeting the Wolbachia cell division protein FtsZ as a new approach for antifilarial therapy. PLoS Negl Trop Dis. 2011.
13. Castillo AL, Osi MO, Ramos JDA, De Francia JL, Dujunco MU, Quilala PF. Efficacy and safety of Tinospora cordifolia lotion in Sarcoptes scabiei var hominis-infected pediatric patients: a single blind, randomized controlled trial. J Pharmacol Pharmacother. 2013;4:39–46.
14. Narkhede RR, Pise A V., Cheke RS, Shinde SD. Recognition of natural products as potential inhibitors of COVID-19 main protease (Mpro): in-silico evidences. Nat Products Bioprospect [Internet]. Nat Prod Bioprospect; 2020 [cited 2021 Nov 10];10:297–306. Available from: https://pubmed.ncbi.nlm.nih.gov/32557405/
15. Liu YT, Hao HP, Xie HG, Lai L, Wang Q, Liu CX, et al. Extensive intestinal first-pass elimination and predominant hepatic distribution of berberine explain its low plasma levels in rats. Drug Metab Dispos [Internet]. Drug Metab Dispos; 2010 [cited 2021 Nov 10];38:1779–84. Available from: https://pubmed.ncbi.nlm.nih.gov/20634337/
16. F, Servi B. New oral delivery system to improve absorption of berberine: likely interaction of cationized chitosan with PG-P pump. undefined. Dr. Yashwant Research Labs Pvt. Ltd.; 2015;5.
17. Spinozzi S, Colliva C, Camborata C, Roberti M, Ianni C, Neri F, et al. Berberine and its metabolites: relationship between physicochemical properties and plasma levels after administration to human subjects. J Nat Prod [Internet]. J Nat Prod; 2014 [cited 2021 Nov 10];77:766–72. Available from: https://pubmed.ncbi.nlm.nih.gov/24593257/
18. Godugu C, Patel AR, Doddapaneni R, Somagoni J, Singh M. Approaches to improve the oral bioavailability and effects of novel anticancer drugs berberine and betulinic acid. PLoS One [Internet]. PLoS One; 2014 [cited 2021 Nov 10];9. Available from: https://pubmed.ncbi.nlm.nih.gov/24614362/
19. Hua W, Ding L, Chen Y, Gong B, He J, Xu G. Determination of berberine in human plasma by liquid chromatography–electrospray ionization–mass spectrometry. J Pharm Biomed Anal Elsevier. 2007;44:931–7.
20. Qin F, Zeng L, Zhu Y, Cao J, Wang X, Liu W. Preparation and evaluation of a timolol maleate drug–resin ophthalmic suspension as a sustained-release formulation in vitro and in vivo. https://doi.org/103109/0363904520151085872 [Internet]. Taylor & Francis; 2015 [cited 2021 Nov 10];42:535–45. Available from: 10.3109/03639045.2015.1085872
21. Lengyel M, Kállai-Szabó N, Antal V, Laki AJ, Antal I. Microparticles, microspheres, and microcapsules for advanced drug delivery. Sci Pharm 2019, Vol 87, Page 20 [Internet]. Multidisciplinary Digital Publishing Institute; 2019 [cited 2021 Nov 10];87:20. Available from: https://www.mdpi.com/2218-0532/87/3/20/htm
22. Alhnan MA, Murdan S, Basit AW. Encapsulation of poorly soluble basic drugs into enteric microparticles: a novel approach to enhance their oral bioavailability. Int J Pharm. Elsevier; 2011;416:55–60.
23. Zhang H, Xu J. Enhanced oral bioavailability of salmeterol by loaded PLGA microspheres: preparation, in vitro, and in vivo evaluation. https://doi.org/103109/107175442014909909 [Internet]. Taylor & Francis; 2014 [cited 2021 Nov 10];23:248–53. Available from: 10.3109/10717544.2014.909909
24. Khan F, Katara R, Ramteke S. Enhancement of bioavailability of cefpodoxime proxetil using different polymeric microparticles. AAPS PharmSciTech [Internet]. Springer; 2010 [cited 2021 Nov 10];11:1368. Available from: /pmc/articles/PMC2974107/.
25. Paolino D, Vero A, Cosco D, Pecora TMG, Cianciolo S, Fresta M, et al. Improvement of oral bioavailability of curcumin upon microencapsulation with methacrylic copolymers. Front Pharmacol [Internet]. Frontiers Media SA; 2016 [cited 2021 Nov 10];7. Available from: /pmc/articles/PMC5174134/.

26. Battu SK, Repka MA, Maddineni S, Chittiboyina AG, Avery MA, Majumdar S. Physicochemical characterization of berberine chloride: a perspective in the development of a solution dosage form for oral delivery. AAPS PharmSciTech [Internet]. Springer; 2010 [cited 2021 Nov 10];11:1466. Available from: /pmc/articles/PMC2974104/.
27. Nitz M, Taranto OP. Film coating of theophylline pellets in a pulsed fluid bed coater. Chem Eng Process Process Intensif [Internet]. Elsevier; 2008 [cited 2021 Nov 10];8:1412–9. Available from: https://www.infona.pl//resource/bwmeta1.element.elsevier-8dbaf593-28b7-39b6-a6a6-fec92b2f8bcf
28. Cao QR, Piao YN, Choi JS, Liu Y, Yang M, Cui JH. Design, in vitro release characterization and pharmacokinetics of novel controlled release pellets containing levodropropizine. Pharm Dev Technol [Internet]. Pharm Dev Technol; 2014 [cited 2021 Nov 10];19:296–303. Available from: https://pubmed.ncbi.nlm.nih.gov/23509871/
29. Bordaweka MS, Zia H, Quadir A. Evaluation of polyvinyl acetate dispersion as a sustained release polymer for tablets. http://dx.doi.org/101080/10717540500313398 [Internet]. Taylor & Francis; 2008 [cited 2021 Nov 10];13:121–31. Available from: 10.1080/10717540500313398
30. Al-Zoubi N, AlKhatib HS, Bustanji Y, Aiedeh K, Malamataris S. Sustained-release of buspirone HCl by co spray-drying with aqueous polymeric dispersions. Eur J Pharm Biopharm [Internet]. Eur J Pharm Biopharm; 2008 [cited 2021 Nov 10];69:735–42. Available from: https://pubmed.ncbi.nlm.nih.gov/18291632/
31. Fini A, Bergamante V, Ceschel GC, Ronchi C, de Moraes CAF. Fast dispersible/slow releasing ibuprofen tablets. Eur J Pharm Biopharm [Internet]. Eur J Pharm Biopharm; 2008 [cited 2021 Nov 10];69:335–41. Available from: https://pubmed.ncbi.nlm.nih.gov/18182280/
32. Kolter K, Dashevsky A, Irfan M, Bodmeier R. Polyvinyl acetate-based film coatings. Int J Pharm Elsevier; 2013;457:470–479.
33. Sutthapitaksakul L, Thanawuth K, Dass CR, Sriamornsak P. Optimized taste-masked microparticles for orally disintegrating tablets as a promising dosage form for Alzheimer's disease patients. Pharm 2021, Vol 13, Page 1046 [Internet]. Multidisciplinary Digital Publishing Institute; 2021 [cited 2021 Nov 10];13:1046. Available from: https://www.mdpi.com/1999-4923/13/7/1046/htm
34. Patole VC, Pandit AP. Mesalamine-loaded alginate microspheres filled in enteric coated HPMC capsules for local treatment of ulcerative colitis: in vitro and in vivo characterization. J Pharm Investig 2017 483 [Internet]. Springer; 2017 [cited 2021 Nov 10];48:257–67. Available from: 10.1007/s40005-017-0304-1
35. Choudhury D, Murty US, Banerjee S. 3D printing and enteric coating of a hollow capsular device with controlled drug release characteristics prepared using extruded Eudragit® filaments. 101080/1083745020211970765 [Internet]. Taylor & Francis; 2021 [cited 2021 Nov 10];26:1010–20. Available from: 10.1080/10837450.2021.1970765
36. Ray S, Banerjee S, Maiti S, Laha B, Barik S, Sa B, Bhattacharyya UK. Novel interpenetrating network microspheres of xanthan gumpoly(vinyl alcohol) for the delivery of diclofenac sodium to the intestine in vitro and in vivo evaluation. Drug Deliv. 2010;17:508–19.
37. Dash S, Murthy PN, Nath L, Chowdhury P. Kinetic modeling on drug release from controlled drug delivery systems. Acta Pol Pharm - Drug Res. 2010;67:217–23.
38. Desai SJ, Simonelli AP, Higuchi WI. Investigation of factors influencing release of solid drug dispersed in inert matrices. J Pharm Sci Elsevier. 1965;54:1459–64.
39. Son GH, Lee BJ, Cho CW. Mechanisms of drug release from advanced drug formulations such as polymeric-based drug-delivery systems and lipid nanoparticles. J Pharm Investig 2017 474 [Internet]. Springer; 2017 [cited 2021 Nov 10];47:287–96. Available from: 10.1007/s40005-017-0320-1
40. Higuchi T, York N. Mechanism of sustained-action medication. Theoretical analysis of rate of release of solid drugs dispersed in solid matrices. J Pharm Sci [Internet]. John Wiley & Sons, Ltd; 1963 [cited 2021 Nov 10];52:1145–9. Available from: 10.1002/jps.2600521210
41. Mathematical models of drug release. Strateg to Modify Drug Release from Pharm Syst. Woodhead Publishing; 2015;63–86.
42. Imre S, Vlase L, Muntean DL. Bioanalytical method validation. Rev Rom Med Lab. 2008;10:13–21.
43. Bordaweka MS, Zia H, Quadir A. Evaluation of polyvinyl acetate dispersion as a sustained release polymer for tablets. Drug Deliv [Internet]. Drug Deliv; 2006 [cited 2021 Nov 10];13:121–31. Available from: https://pubmed.ncbi.nlm.nih.gov/16423800/
44. Zoubari G, Ali R, Dashevskiy A. Water-insoluble polymers as binders for pellet drug layering: effect on drug release and performance upon compression. Int J Pharm [Internet]. Int J Pharm; 2019 [cited 2021 Nov 10];569. Available from: https://pubmed.ncbi.nlm.nih.gov/31362093/
45. Al-Zoubi N, Al-obaidi G, Tashtoush B, Malamataris S. Sustained release of diltiazem HCl tableted after co-spray drying and physical mixing with PVAc and PVP. Drug Dev Ind Pharm [Internet]. Drug Dev Ind Pharm; 2016 [cited 2021 Nov 10];42:270–9. Available from: https://pubmed.ncbi.nlm.nih.gov/26035331/
46. Li-Fang F, Wei H, Yong-Zhen C, Bai X, Qing D, Feng W, et al. Studies of chitosan/Kollicoat SR 30D film-coated tablets for colonic drug delivery. Int J Pharm [Internet]. Int J Pharm; 2009 [cited 2021 Nov 10];375:8–15. Available from: https://pubmed.ncbi.nlm.nih.gov/19457627/
47. Dinarvand R, Mahmoodi S, Farboud E. Effect of process variables on particle size of gelatin microspheres containing lactic acid. Pharm Dev Technol [Internet]. Pharm Dev Technol; 2004 [cited 2021 Nov 10];9:291–9. Available from: https://pubmed.ncbi.nlm.nih.gov/15458234/
48. Ofokansi KC, Kenechukwu FC, Isah AB, Okigbo EL. Formulation and evaluation of glutaraldehyde-crosslinked chitosan microparticles for the delivery of ibuprofen. Trop J Pharm Res [Internet]. University of Benin; 2013 [cited 2021 Nov 10];12:19–25. Available from: https://www.ajol.info/index.php/tjpr/article/view/86169
49. Zhang Y, Cui YL, Gao LN, Jiang HL. Effects of β-cyclodextrin on the intestinal absorption of berberine hydrochloride, a P-glycoprotein substrate. Int J Biol Macromol. 2013.
50. Zhaojie M, Ming Z, Shengnan W, Xiaojia B, Hatch GM, Jingkai G, Li C. Amorphous solid dispersion of berberine with absorption enhancer demonstrates a remarkable hypoglycemic effect via improving its bioavailability. Int J Pharm. Elsevier. 2014;467:50–9.
51. Nayak UY, Gopal S, Mutalik S, Ranjith AK, Reddy MS, Gupta P, et al. Glutaraldehyde cross-linked chitosan microspheres for controlled delivery of zidovudine. J Microencapsul [Internet]. J Microencapsul; 2009 [cited 2021 Nov 10];26:214–22. Available from: https://pubmed.ncbi.nlm.nih.gov/18819029/
52. Genta I, Costantini M, Asti A, Conti B, Montanari L. Influence of glutaraldehyde on drug release and mucoadhesive properties of chitosan microspheres. Carbohydr Polym Elsevier. 1998;36:81–8.
53. Manoharan C, Singh J. Insulin loaded PLGA microspheres: effect of zinc salts on encapsulation, release, and stability. J Pharm Sci [Internet]. J Pharm Sci; 2009 [cited 2022 Jan 20];98:529–42. Available from: https://pubmed.ncbi.nlm.nih.gov/18548615/
54. Aamir MN, Ahmad M. Production and stability evaluation of modified-release microparticles for the delivery of drug combinations. AAPS PharmSciTech. 2010;11:351–5.
55. Puthli S, Vavia PR. Stability studies of microparticulate system with piroxicam as model drug. AAPS PharmSciTech. 2009;10:872–80.
56. Wikarsa S, Durand D, Delarbre JL, Baylac G, Bataille B. The improvement of ibuprofen dissolution rate through microparticles spray drying processed in an aqueous system. Drug Dev Ind Pharm. 2008;34:485–91.

57. Jia J, Zhang K, Zhou X, Ma J, Liu X, Xiang A, Ge F. Berberine-loaded solid proliposomes prepared using solution enhanced dispersion by supercritical CO2: sustained release and bioavailability enhancement. J Drug Deliv Sci Technol Elsevier; 2019;51:356–363.
58. Chen W, Fan D, Meng L, Miao Y, Yang S, Weng Y, He H, Tang X. Enhancing effects of chitosan and chitosan hydrochloride on intestinal absorption of berberine in rats. Drug Dev Ind Pharm. 2012;38:104–10.
59. Chen W, Miao YQ, Fan DJ, Yang SS, Lin X, Meng LK, Tang X. Bioavailability study of berberine and the enhancing effects of TPGS on intestinal absorption in rats. AAPS PharmSciTech. 2011;12:705–11.
60. Shi C, Tong Q, Fang J, Wang C, Wu J, Wang W. Preparation, characterization and in vivo studies of amorphous solid dispersion of berberine with hydrogenated phosphatidylcholine. Eur J Pharm Sci [Internet]. Elsevier B.V.; 2015;74:11–7. Available from: 10.1016/j.ejps.2015.04.001